

Vibratory Load Predictions of a High-Advance-Ratio Coaxial Rotor System Validated by Wind Tunnel Tests

Roland Feil *

Jürgen Rauleder †

Manfred Hajek ‡

Institute of Helicopter Technology
Technical University of Munich, Germany

To investigate the aeromechanics of coaxial counter-rotating lift-offset rotor systems, a comprehensive analysis model of a laboratory-scale torque-balanced rotor designed for high-advance-ratio forward flight was developed. Measured blade and control system geometries and structural properties were input to the model. Lower-order aerodynamics modeling with a free vortex wake method was used. While previous analytical studies on this coaxial rotor test rig have focused on performance and control requirements, in this current work, vibratory hub and pitch link loads, the influence of rotor-rotor phasing and the effects on blade deflections and tip clearance were investigated. The analysis was validated by wind-tunnel tests at advance ratios of 0.21–0.52 and for a lift offset varying from zero to 25%. Coaxial rotor performance, pitch link loads, unsteady thrust and rolling moments correlated well with the measurements. Pitching and rolling moment 2/rev and 4/rev harmonics correlated well for all lift offsets and advance ratios, whereas the vibratory torque was significantly overpredicted. The correct trends for varying lift offset and advance ratio were predicted in drag, side force, and thrust harmonics. Corresponding magnitudes were also predicted well, although an underprediction of the side force 4/rev harmonics was observed. Good correlation was found for the predicted blade tip clearance between the rotors over the entire range of lift offset and rotor-rotor phase angles, showing that advance ratio had little effect and judicious use of rotor phasing can increase the critical tip clearance.

NOMENCLATURE

CAMRAD II	Comprehensive Analytical Model of Rotorcraft Aerodynamics and Dynamics	c	rotor blade chord, m
C_{MX}	rotor rolling moment coefficient, $M_X/(\rho\pi\Omega^2R^5)$	n	index for rotor n /rev harmonics
C_{MY}	rotor pitching moment coefficient, $M_Y/(\rho\pi\Omega^2R^5)$	r_{rc}	radial station of root cutout, m
C_Q	rotor torque coefficient, $Q/(\rho\pi\Omega^2R^5)$	z_R	design inter-rotor spacing, m
C_T	rotor thrust coefficient, $T/(\rho\pi\Omega^2R^4)$	z_{tip}	rotor blade tip displacement, m
C_X	rotor drag coefficient, $F_X/(\rho\pi\Omega^2R^4)$	Δz_{tip}	coaxial rotor blade tip clearance, m
C_Y	rotor side force coefficient, $F_Y/(\rho\pi\Omega^2R^4)$	β_p	precone angle, deg
F_{PL}	pitch link forces, N	$\Theta_0, \Theta_{1s}, \Theta_{1c}$	collective and cyclic controls, deg
F_Z	rotor axial force, N	μ	advance ratio, $V_\infty/(\Omega R)$
L/D_e	Lift-to-equivalent-drag ratio	ρ	air density, kg/m^3
LO	lift offset	σ	rotor solidity, $N_b c/(\pi R)$
M_X	rotor rolling moment, Nm	Φ	rotor-rotor phase angle, deg
N_b	number of rotor blades	Ψ_b	rotor blade azimuth angle, deg
R	rotor radius, m	Ω	rotor angular velocity, rad/s
U, L	Upper and Lower rotor index superscript		
V_{tip}	rotor blade tip speed, ΩR , m/s		

1. INTRODUCTION

Helicopter configurations using coaxial, counter-rotating rotor systems have recently been enjoying revived interest [1]. The reasons for this are mostly their compactness, i.e., minimized footprint making them more suitable for congested operating environments (such as in cities [2] or on ship decks), and good overall efficiency by saving the additional power needed for the tail rotor (that is needed for torque-balancing the main rotor system). However, coaxial rotor systems are not a panacea either, because the aerodynamic interactions between the rotors can have a variety of sometimes detrimental effects on system performance,

* Graduate Research Assistant. roland.feil@tum.de

† Lecturer. juergen.rauleder@tum.de

‡ Professor and Department Head. hajek@tum.de

Presented at the 43rd European Rotorcraft Forum, Milano, Italy, September 12–15, 2017. Copyright ©2017 by the authors except where noted. All rights reserved. Published by CEAS with permission.

structural loads, or noise emissions. These interactional aeromechanics are yet not well understood, and so it has been mostly unclear how exactly the upper rotor affects the lower rotor and vice versa.

Current VTOL aircraft compromise between efficient hover performance and forward flight performance. With both high-speed capability and range being important future requirements, the aforementioned compromise is even more of a challenge. Whereas tiltrotor aircraft have extended range and good high-speed performance, their hover performance is, in general, inferior to that of conventional helicopters or compound helicopters because of their high disk loading [3]. Conversely, fast edgewise flight of conventional helicopter designs is mainly limited by the asymmetric aerodynamics at the rotor disk and associated retreating blade stall.

One concept to overcome these forward flight speed limitations imposed by the dynamic stall on the retreating side of the rotor disk is by off-loading the retreating blade from its requirement to balance the lift that is being generated on the advancing side of the rotor disk, i.e., to allow non-zero roll moments at the individual rotors. In this way, the full lift potential of the advancing blade can be realized, allowing it to operate at angles of attack closer to the optimum, therefore also attaining better performance at high forward flight speeds or high advance ratios. This can be accomplished by two counter-rotating rotors in a coaxial configuration (see Fig. 1), such that most of the lift is produced by the advancing blades of each individual rotor while maintaining roll moment trim of the entire rotor system and aircraft (because the individual rotor rolling moments balance out each other). Such coaxial rotor systems designed for high advance ratios have gained increased attention in recent years, up to the point of full-scale technology demonstrators like, e.g., the X2 from Sikorsky [4–7].

A comprehensive overview of previous experimental work on coaxial rotors until 1997 is given by Coleman [8]. Ramasamy [9] conducted a more recent experimental study on the influence of interactional aerodynamics on the power requirements for a number of different rotor systems, including tandem, side-by-side, and coaxial rotors. However, the majority of the work on coaxial rotor systems utilizing lift offset has been done using analytical models of various levels of fidelity. A fidelity level analysis of such models and the effects on the predictions are reported in [10], including validation by laboratory (model-scale) rotor test data.

Comprehensive analysis has been used to include the effects of structural dynamics using lower-order aerodynamics modeling, and so investigate the effects that lift offset and blade loading have on the rotor performance [11, 12]. Coupled computational fluid dynamics/computational structural dynamics (CFD/CSD) analyses have also been conducted [13, 14] using higher-order CFD modeling (mostly unsteady Reynolds-averaged Navier–Stokes, URANS) for the aerodynamics, together

with comprehensive rotor codes to solve for the blade motions and the structural dynamics such as elastic blade deformations. However, higher-order aerodynamics modeling does not necessarily improve the correlation to measurements [14] and any numerical prediction still needs validation by well-controlled experiments.

Model-scale experiments have been performed for a high-advance-ratio 2-by-2 bladed coaxial rotor system in hover [15–18] and in forward flight [19] using the Glenn L. Martin Wind Tunnel at the University of Maryland; see Fig. 1). Furthermore, comprehensive analysis has been done for the same (approximately 2m-diameter) rigid coaxial rotor system [20–24]. Focusing on the effects from blade crossings, additional studies investigated the transient loads and blade deformations in a 1-by-1 bladed coaxial rotor system during hover by both analysis and experiments [25]. Further comprehensive analysis for different coaxial rotor systems were also done by Yeo et al. [26], by using other codes, such as RCAS, which previously showed excellent agreement with CAMRAD II for tiltrotor models [27].

Rigid rotors are one key technology enabler for coaxial rotor systems that are designed for high forward flight speeds [1]. The significantly reduced flapping motion of the rotor blades allows for smaller rotor spacing (reducing the hub drag) and also enables lift offset [5, 6]. However, steady and unsteady airloads, and the increased vibratory forces and moments that are produced by such rigid rotors are directly transmitted to the hub, pitch links, and other components. Therefore, these effects need to be well understood to be able to design such rotor systems against, e.g., structural fatigue of the aforementioned mechanical components. Furthermore, aerodynamic interactions between the upper and lower rotors, blade deflections and, in particular, their effects on blade clearance need to be investigated further, and this is particularly important for rotor systems designed with a small rotor–rotor spacing (for hub drag reduction).

To this end, in the present work, a comprehensive modeling effort is discussed, also showing correlations with model-scale wind-tunnel tests to validate the modeling approach. A detailed level of structural dynamics modeling of the rotor blades was used with a comprehensive analysis including lower-order aerodynamics, namely a free vortex wake (FVW) method, to ensure computational efficiency. This fast and efficient modeling approach without the need to use high-performance computing facilities will enable quick analyses and parameter sweeps in the design stage. The predictive model was validated in forward flight at several advance ratios of up to 0.52 and lift offsets of up to 25% by comparing to the measurements that were obtained with a coaxial 2m-diameter rigid model rotor in the Glenn L. Martin Wind Tunnel at the University of Maryland. While previous modeling efforts focused on performance and controls, the focus of this current work is on the combined effects of advance ratio and lift offset on the

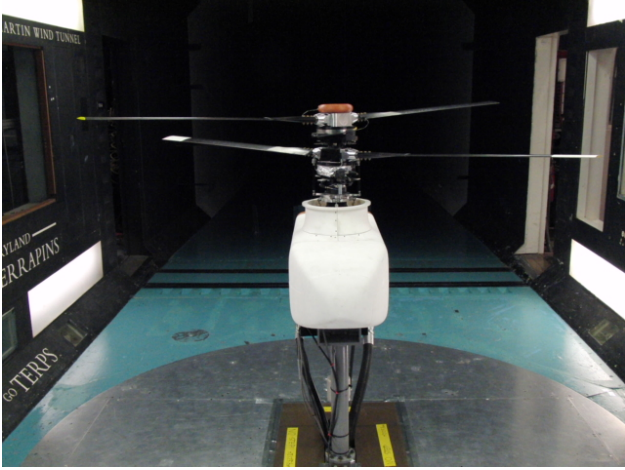


Fig. 1: 2-by-2 bladed coaxial rotor system in the Glenn L. Martin Wind Tunnel at the University of Maryland [19].

vibratory hub and pitch link loads, and also on the investigation of rotor–rotor phasing and blade tip clearance.

2. DESCRIPTION OF THE EXPERIMENTS

Experiments were performed on a 2m diameter, rigid coaxial, counter-rotating rotor system; see Fig. 1. Details of the experimental setup are given in Refs. [16–20] and a summary of the rotor dimensions and operational parameters is given in Tab. 1, the control system parameters in Tab. 2 and Fig. 2, and the elastic blade characteristics in Fig. 3. Data from both hover and wind tunnel tests, performed by Cameron et al. [16–19], were used to calibrate and validate the numerical model. Steady and vibratory hub loads, pitch link loads, blade pitch angles as well as blade tip clearance were measured at over 400 test conditions, up to an advance ratio of 0.52 and a maximum lift offset of nearly 25% including varying rotor–rotor phasing.

Table 1: Rotor parameters.

Parameter	2-bladed	Coaxial
N_b	2	2×2
R , m	1.016	1.016
r_{rc} , m	0.122	0.122
z_R , m	-	0.140 m (13.8 % R)
Airfoil section	VR-12	VR-12
β_p , deg	3	3
c , m	0.080	0.080
σ	0.05	0.1 (total)
V_{tip} , m/s	95.8	95.8
Ω , RPM	900	900

3. MODELING APPROACH

A comprehensive analysis of the presented rotor configuration was performed using CAMRAD II [28], an aeromechanics analysis tool for rotorcraft that incorporates a

Table 2: Control system parameters.

Parameter	Upper Rotor	Lower Rotor
Pitch horn length, m	0.013	0.0348
Pitch link stiffness, N/m	7.0×10^5	7.3×10^5
Axial pitch link length, m	0.873	0.1625

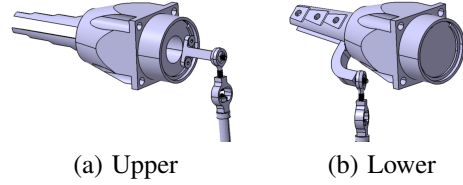


Fig. 2: Upper and lower rotor pitch link geometries.

combination of advanced treatments of rotating systems, including multibody dynamics, nonlinear finite element methods, and rotorcraft aerodynamics models. In this study, the rotor blade aerodynamics were modeled based on lifting line theory using steady two-dimensional airfoil characteristics. These airfoil characteristics of the VR-12 airfoil section were obtained from CFD computations for multiple Mach numbers and were in good agreement with experimentally measured rotor thrust and power [23].

The aerodynamics model consisted of 22 aerodynamic panels along with 16 structural beam elements per blade. Unless otherwise noted, 24 azimuthal positions were calculated per rotor revolution. A computationally efficient free vortex wake (FVW) method was used to compute the rotor wake including interaction between the wakes of the two rotors. The free wake method discretizes the rotor wake into vortex filaments and then calculates the velocities induced by the filaments on each other, and on the flow field, using the Biot–Savart law [29, 30].

In the current FVW analysis, a multiple trailer model with two trailers and vortex roll-up was used that previously showed good predictions of the lift distribution, vibrations, and tip vortex geometry [31]. Bagai–Leishman’s vorticity distribution [32], a Bagai–Leishman vortex core radius growth model [29] and a general free wake geometry allowed rotor–rotor interactions to be accounted for. In order to sufficiently account for any form of blade–vortex or vortex–vortex interaction that affects the results, the near wake was truncated after 60° of wake age and the far wake was truncated after ten rotor revolutions of wake age with the wake’s distortion being extended by another five rotor revolutions. The shed wake was accounted for only in forward flight conditions.

The rotor and control system parameters of the experimental setup and the CAMRAD II model were identical; see Tabs. 1, 2 and Figs. 2, 3. In the numerical model, elastic pitch links were used to account for the combined torsional stiffness of the rotor blade and pitch control mechanism. The pitch link elasticities are shown in Tab. 2 and the geometric parameters of the pitch control system can be visualized with Fig. 2. These (scaled) rotor parameters

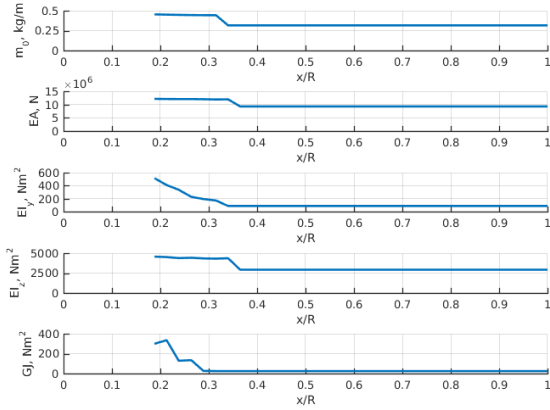


Fig. 3: Rotor blade spanwise structural properties.

(see Tab. 1) are similar to those of the Sikorsky X2 technology demonstrator [4–7], that successfully demonstrated high-advance-ratio flight. Therefore, the current setup is well suited to perform aeromechanics model validation of a coaxial rotor model designed for fast forward flight.

Measurements obtained with the previously described experimental setup were used to validate the numerical model [16, 20]. This setup included a cuffed (and thus stiffer) blade geometry for the inboard sections. The structural properties of the rectangular and non-twisted composite blades were measured by static blade bending tests; see the distribution of measured values of the blade section mass m_0 , the axial stiffness EA , the flapwise and lagwise bending stiffness EI_Y and EI_Z , and the torsional stiffness GJ in Fig. 3. Blade sectional parameters at the blade grip (between root cutout outboard location at $0.12R$ and $0.19R$) were adjusted accordingly in order to match the non-rotating natural frequencies with measured data. This is a reasonable and physics-based assumption because, for mounting purposes, the blade had three holes at the inboard sections (see Fig. 2) decreasing, e.g., the lag stiffness accordingly.

In order to account for the finite stiffness of the blade mounting in flap direction during testing, the according inboard elasticities at the root cutout section ($0R$ to $0.12R$) were adjusted in flap direction in the modeling by matching the 1st flap frequency; see Fig. 4. This improved the model compared to previous analysis [20]. It is a more realistic representation of the physics because the actual blade mounting of the wind tunnel test rig was more compliant compared to the rigid static testing that was used for the detection of the blade non-rotating natural frequencies. The current approach also incorporated effects from, e.g., free play in the blade mountings that may also affect the resulting blade deflections [20].

Resulting natural frequencies were validated against experimental test data for the first three flap (F), the first lag (L) and the first torsion (T) modes; see Fig. 6. Coaxial and isolated upper and lower rotor hover performance predictions were previously validated against experimental data

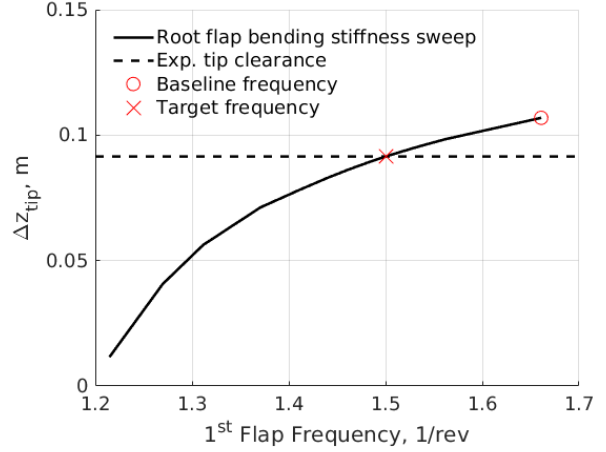


Fig. 4: Coaxial rotor tip clearance study with varying root flap bending stiffness that is reflected by the 1st flap frequency at $\Theta_0=8^\circ$, 17% LO, and $\mu=0.31$.

[20]. Furthermore, isolated and coaxial rotor characteristics with varying blade loadings and increasing advance ratios agreed well with the experiments [20]. However, pitch link and vibratory hub load measurements were, at the stage of previous analysis, not available for the whole range of operating advance ratios and lift offsets. The following discussion includes some of these new results and it also includes more experimental and numerical analysis on the vibratory hub loads and the control system loads over the full range of operating conditions, including the effect of phase variation between the rotors.

During hover, a six degree of freedom trim was used that is described in more detail in Refs. [20, 21]. For the current coaxial configuration in forward flight, a five-degree-of-freedom wind tunnel trim was used that independently varied the collective of the lower rotor and both cyclic controls of the upper and the lower rotors. The upper rotor collective control was set as input for the wind tunnel trim condition and the other trim parameters were adjusted according to the flight condition. This trim algorithm provided the capability to individually target particular isolated rotor loads as well as total system loads, and it is the same control strategy as used in the experiments. The five residuals for the coaxial trim algorithm were torque balance and independent pitch and roll moments for each rotor. The trim convergence criteria was set to less than 0.1%.

Lift offset, LO, is illustrated in Fig. 5 with the thrust vector of an individual rotor being shifted outboard when lift offset is applied. Lift offset was defined by

$$LO = \frac{|C_{MX}^U| + |C_{MX}^L|}{C_T^U + C_T^L} \quad (1)$$

for the (total) coaxial rotor system, where C_T is the thrust coefficient and C_{MX} is the roll moment coefficient of each

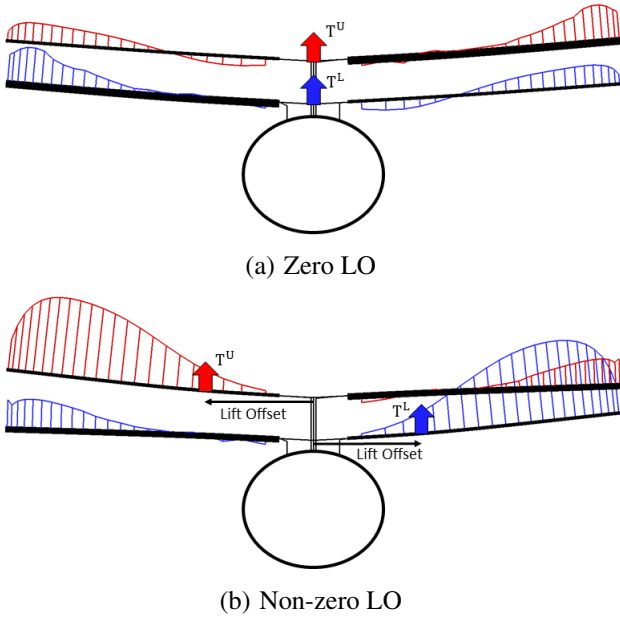


Fig. 5: Illustration of lift offset with thrust distributions on a coaxial rotor with and without LO (view from nose to tail).

individual rotor.

The upper rotor rotates in counter-clockwise and the lower rotor rotates in clockwise direction when viewed from above. Figure 5 furthermore shows the increased elastic blade flap bending resulting from the thrust vectors being shifted to the advancing sides for increased lift offsets.

4. RESULTS AND DISCUSSION

Natural frequencies

Figure 6 shows the fan plot including the measured non-rotating natural frequencies and numerical results for the whole range of rotational speeds. Validation was performed according to the test environment that excluded control system elasticities. The numerical results using CAMRAD II agreed well with the experimental data; see Fig. 6.

Also accounting for the appropriate control system geometries and representative elasticities (see Tab. 2), the respective predicted natural frequencies were added in Fig. 6 (dashed lines in red for the upper and lower rotor). Control system elasticities primarily affected the feathering axis, and hence the torsional mode and the respective natural frequencies. Both the lower and the upper rotor torsional frequencies were reduced, with a more significant effect on the upper rotor control system because of the relatively small pitch horn length of the upper rotor pitch rods; see Tab. 2 and Fig. 2.

Table 3 shows the natural frequency data from measurements for each mode and the according standard deviations. The table also includes the CAMRAD II results for

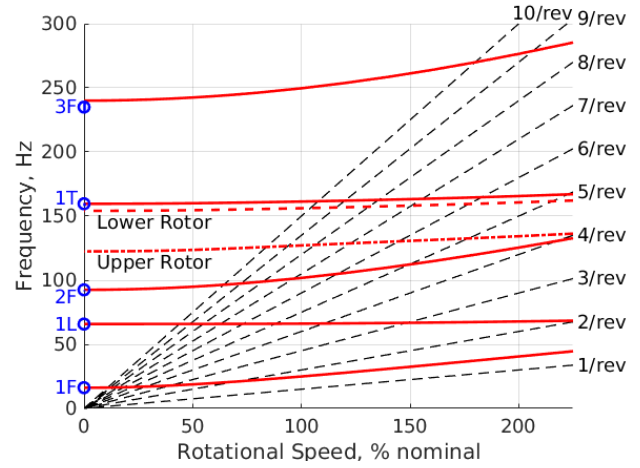


Fig. 6: Predicted fan plot, calibrated by measured non-rotating blade natural frequencies, shown as open circles (dashed lines include control system elasticities).

the validated non-rotating condition (0 RPM), the nominal operational speed (900 RPM), and also a high-speed case of 1800 RPM, which is a test condition that was used for previous measurements that are not reported in the current work. Table 3 also shows the predicted 1st torsional natural frequency of the upper and lower rotor blades with elastic pitch links.

Lift-to-drag ratio

Because hover performance as well as a wide range of wind tunnel performance data including variations for lift offset, advance ratio and collectives were previously evaluated in Ref. [20], here only the coaxial rotor lift-to-drag ratios are shown. Figure 7 shows the lift-to-drag ratio versus advance ratio and Fig. 8 versus lift offset. The rotor lift-to-drag ratio is defined [32] by

$$L/D_e = \frac{C_T}{\frac{C_Q}{\mu} + C_X} \quad (2)$$

with C_T being the rotor's thrust coefficient, C_Q the torque coefficient, μ the advance ratio, and C_X the rotor drag coefficient. For the combined coaxial rotor system, the numerical results were in good agreement with the experimental data, although the individual upper and lower rotor L/D_e magnitudes differed much more from each other in the test data compared to the numerical results. The CAMRAD model captured this effect at very high speeds ($\mu > 0.5$) where not only the coaxial but also the individual upper and lower rotor lift-to-drag ratios correlated well; see Fig. 8. An increasing advance ratio showed an increasing lift-to-drag ratio until a performance maximum was reached, and it decreased again at higher speeds; see Fig. 7. Notice that the best performance occurred at higher advance ratios for increasing collectives.

Table 3: Modal Frequencies, in Hz, for a rigid control system except where noted.

Mode	Exp. freq. 0 RPM	Exp. standard deviation 0 RPM	CAMRAD II 0 RPM	CAMRAD II 900 RPM (100 % nominal)	CAMRAD II 1800 RPM (200 % nominal)
1 st Flap	16.2	± 0.20	16.13	24.91 (1.66/rev)	40.51 (1.35/rev)
1 st Lag	65.8	-	65.79	66.09 (4.40/rev)	67.79 (2.26/rev)
2 nd Flap	92.5	±0.50	92.49	101.77 (6.78/rev)	125.45 (4.18/rev)
1 st Torsion	159.6	±1.00	159.70	161.45 (10.76/rev)	165.71 (5.52/rev)
1 st Torsion (elastic upper PL)	-	-	122.50	126.13 (8.41/rev)	133.46 (4.45/rev)
1 st Torsion (elastic lower PL)	-	-	154.10	155.92 (10.39/rev)	160.47 (5.35/rev)
3 rd Flap	235	± 5.00	240.00	249.64 (16.64/rev)	276.53 (9.22/rev)

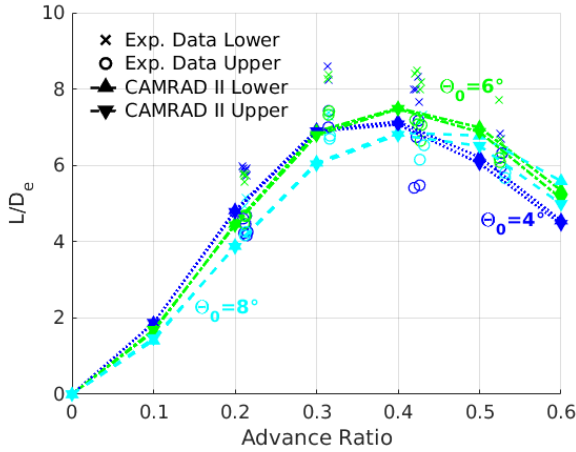


Fig. 7: Coaxial rotor lift-to-drag ratio versus advance ratio for zero LO and multiple collectives.

The variation of lift offset (see Fig. 8) also showed maxima of L/D_e . At higher speeds, the off-loading from the re-treating blade becomes more effective, and so the lift offset becomes more advantageous. It also shows that up to an advance ratio of $\mu = 0.21$, the effect of lift offset decreases the rotor's performance. Hence, lift offset may only have a positive impact on the performance above a certain advance ratio, which was greater than $\mu = 0.21$ for the current configuration.

Pitch link loads

Fig. 9 shows the variation of pitch bearing damping ratios for a validation of the 1/rev pitch link harmonics. The experimental data showed increased 1/rev characteristic magnitudes for the movement around the feathering axis. This is because of increased damping due to the grease in the pitch bearings. In order to sufficiently compensate for this effect, this numerical study (Fig. 9) shows the effects from varying pitch bearing damping ratios in the CAMRAD II model in comparison to two experimental data sets (i.e., two test cases under identical operating conditions). The first ten harmonics were included to show that the pitch damping primarily affected the 1/rev harmonics, and only slightly influenced some of the higher harmonics, such as

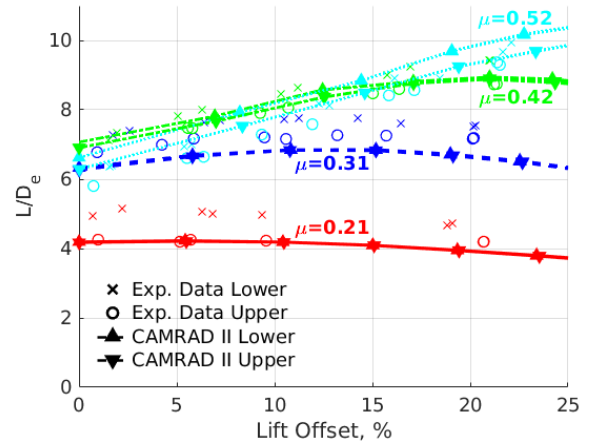


Fig. 8: Coaxial rotor lift-to-drag ratio versus LO at $\Theta_0 = 8^\circ$ for multiple advance ratios.

the 8/rev harmonics.

The shown test condition was for an advance ratio of $\mu = 0.31$ and an upper rotor collective pitch, Θ_0 , of 8° . Because of the difference in (upper and lower) rotor control system geometries (see Tab. 2 and Fig. 2), the lower rotor (not shown) had reduced magnitudes in the 1/rev pitch link forces. However, the characteristics with varying pitch damping were identical to the upper rotor because the same bearings were used. The numerical study showed that a pitch-bearing-induced damping of 0.03 Nms/rad was the most accurate. Therefore, this damping was used to model both the upper and the lower rotor in the subsequent analyses.

Figure 10 examines the pitch link loads harmonic contents (1/rev – 4rev) with varying advance ratio and Fig. 11 shows the phase-averaged pitch link loads (mean removed) in the time domain at three different advance ratios. Notice that the shaded area in the phase-averaged loads indicates data scatter over 100 rotor revolutions that were used to obtain phase-averaged results from the experiment [18, 20].

In general, the following numerical results used a lift offset resolution of 5 – 8% (depending on the individual advance ratio) corresponding to a stepwise increasing rolling moment coefficient of $\Delta C_{MX} = 10$. Numerical results in the time domain were reconstructed by using the first 10

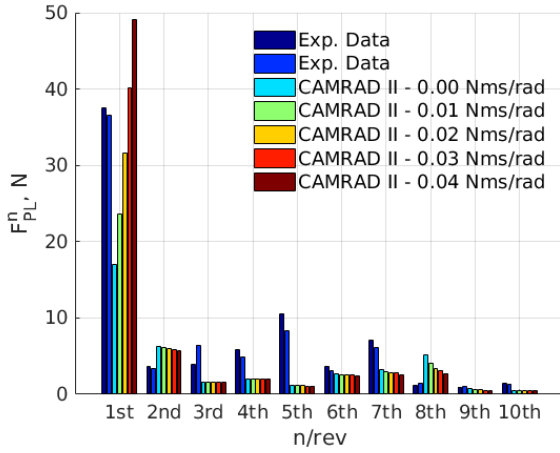


Fig. 9: Upper coaxial rotor pitch link load harmonic magnitudes for varying pitch bearing damping at $\Theta_0 = 8^\circ$, $\mu = 0.31$, and $\Phi = 0^\circ$.

harmonic responses and visualized with 1 deg in azimuth of accuracy.

Figure 11 shows that the resulting 1/rev peak locations (i.e., the phasing) correlated well with the measurements for 0%, 10%, and 20% lift offset. The 1/rev pitch link force characteristics can also be seen from Fig. 10, where both the lower and the upper rotors 1/rev magnitudes in the pitch link loads correlated well with the test data. The amplitudes of the dominating 1/rev harmonics decreased with increasing lift offset for both the upper and the lower rotor because of the off-loading of the retreating blade with larger lift offsets. By that, the retreating blade must no longer achieve such high angles of attack in order to counteract the lift that is produced on the advancing side.

The effect of off-loading the retreating blade can also be seen in Fig. 12 where the numerically determined angles of attack for both the upper and the lower rotor are shown for three lift offset conditions. The area of high angles of attack on the retreating blade reduced with increasing lift offset. A more evenly distributed angle of attack over the rotor disk results in decreased 1/rev load harmonics for an improved lift offset setting. Note that according to the equations of motion, not only the aerodynamics but also the blade inertias, torsional dampings and torsional elasticities affect the resulting pitch link dynamics, which was accounted for in the analysis. At the currently investigated free stream Mach number of about 0.1, the VR-12 airfoil showed effects from blade stall starting from about 11° of angle of attack [22]. Hence, with increasing lift offset also the areas decreased where blade stall occurred; see Fig. 12).

Figure 10 also shows that besides the 1/rev, the other predicted pitch link load harmonics (2/rev – 4/rev) correlated well with the experiments. Only the 3/rev harmonics showed slight underprediction compared to the test data, and these were greater for the upper rotor. This outcome resulted from higher harmonic content in the experimental

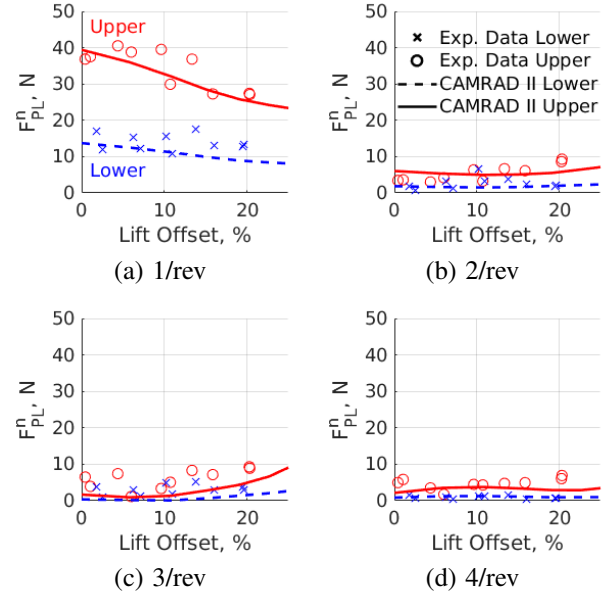


Fig. 10: Harmonic pitch link load magnitudes at $\Theta_0 = 8^\circ$, $\mu = 0.31$, and $\Phi = 0^\circ$.

data compared to the CAMRAD II results; see also Fig. 11. This is because of the free play in the pitch control system of the test rig [20].

Hub loads

Figures 13 and 14 show the axial hub loads and the resulting rotor rolling moments as a function of azimuth for the upper and the lower rotors at three lift offset conditions, for an advance ratio of $\mu = 0.31$ and an upper rotor collective pitch of $\Theta_0 = 8^\circ$ (the lower rotor collective is then found from the required torque balance). Figures 15 – 20 show the hub forces and moments content in the frequency domain for (a) 2/rev and (b) 4/rev results from both numerics and experimental data in all three directions, respectively. Included is the entire range of lift offsets (0% – 25%) and advance ratios (0.21 – 0.52) that were tested in the wind tunnel with an upper rotor collective pitch set to $\Theta_0 = 8^\circ$.

Figure 13 shows that the phasing and the magnitudes of the rotor axial forces (or thrust) over one rotor revolution correlated well with the measurements for zero and medium (represented here by 10% LO) lift offset conditions. With lift offset increasing further, the measured data showed increasing higher-frequency and uneven (especially 1/rev) frequency content. These effects can at least in part be explained by dissimilarities between the blades in terms of mass distribution resulting in a slight rotor imbalance that produced additional harmonics in the experiments. Furthermore, it was difficult to visually track the blades because the rigid rotor hub and the stiff rotor blades resulted in small tip deflections [20]. Therefore, neither magnitude nor phase correlated well for this high lift offset condition of LO = 20%. CAMRAD II shows that the 4/rev content from rotor-rotor interactions becomes the dominating dynamics of the rotor axial forces with increasing

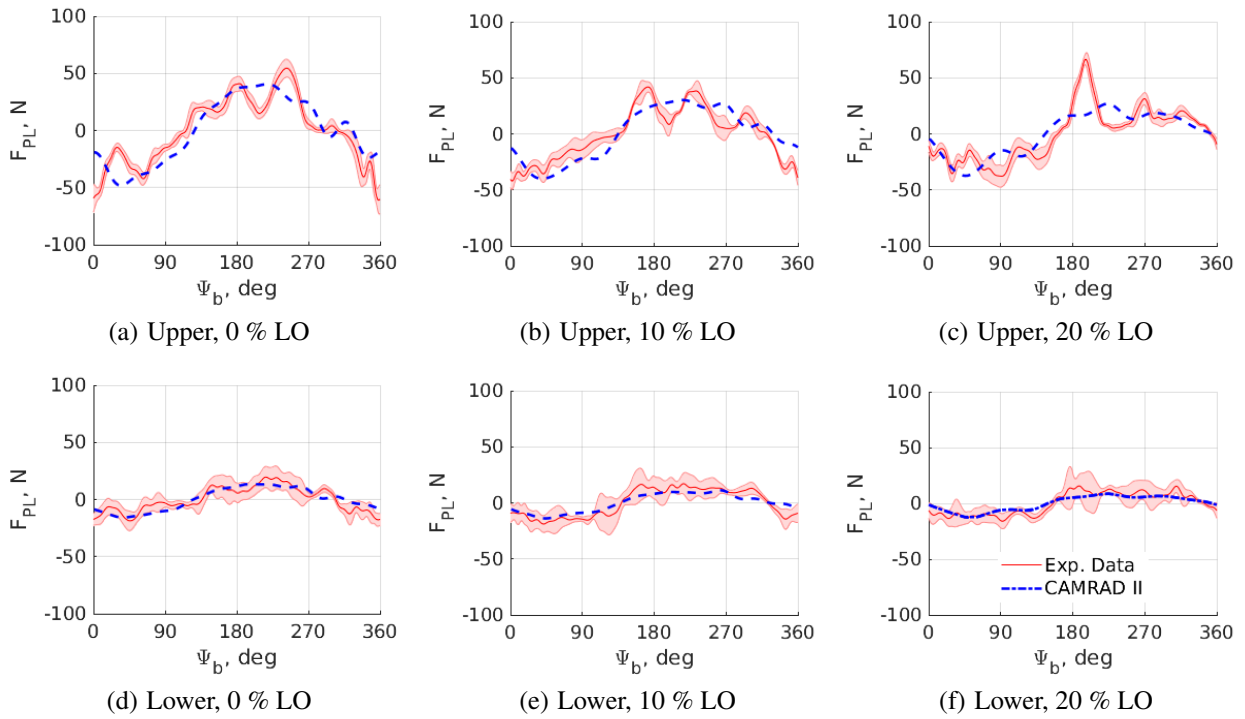


Fig. 11: Pitch link forces, F_{PL} , (mean removed) at $\Theta_0 = 8^\circ$, $\mu = 0.31$, and $\Phi = 0^\circ$ for three different lift offsets.

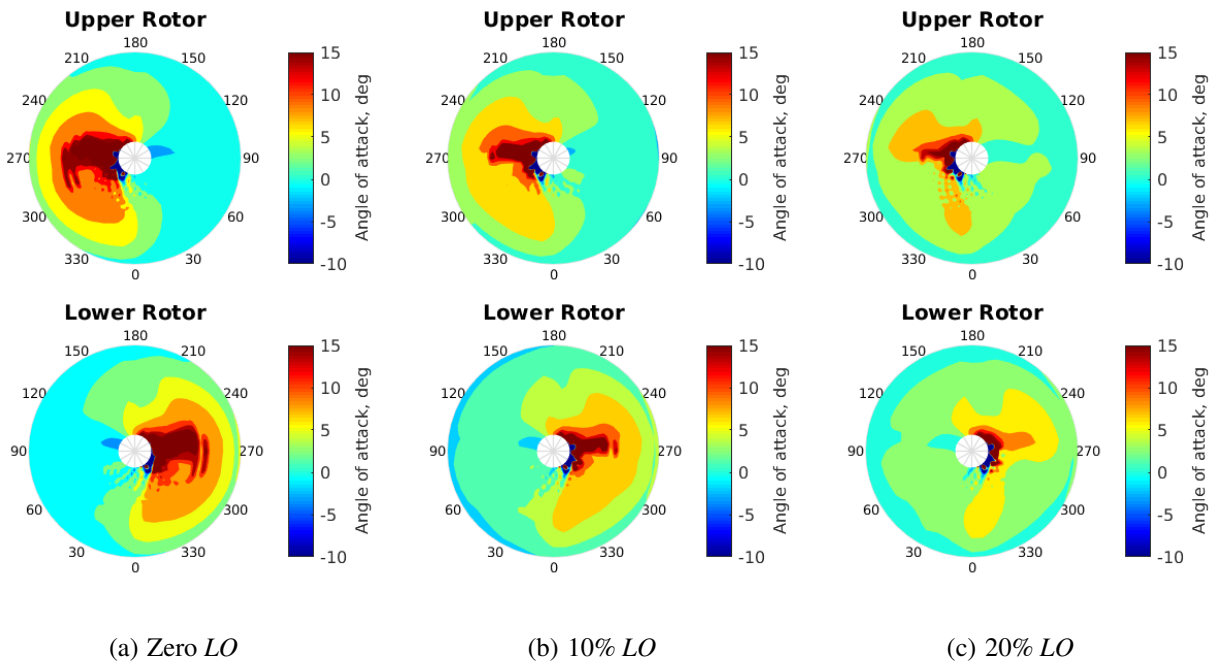


Fig. 12: Upper and lower rotor angles of attack for the reference blade of each rotor at $\Theta_0 = 8^\circ$, $\mu = 0.31$, and $\Phi = 0^\circ$ for three different lift offsets.

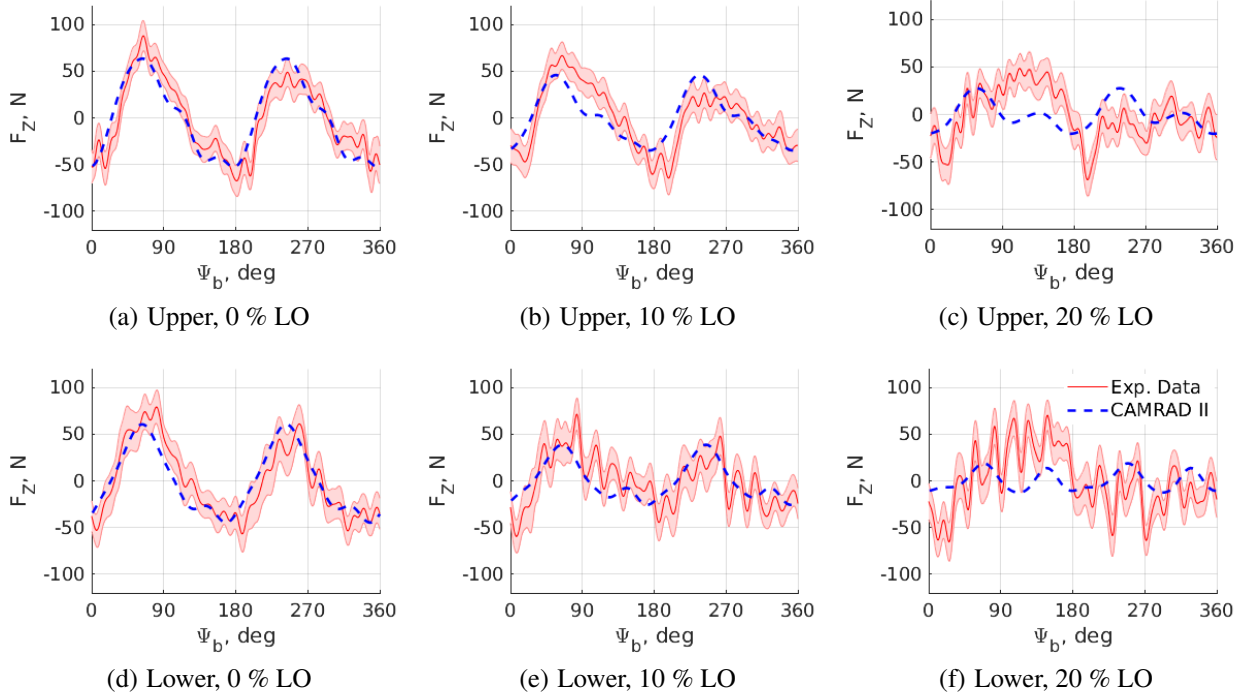


Fig. 13: Rotor axial forces, F_z , (mean removed) at $\Theta_0 = 8^\circ$, $\mu = 0.31$, and $\Phi = 0^\circ$ for three different lift offsets.

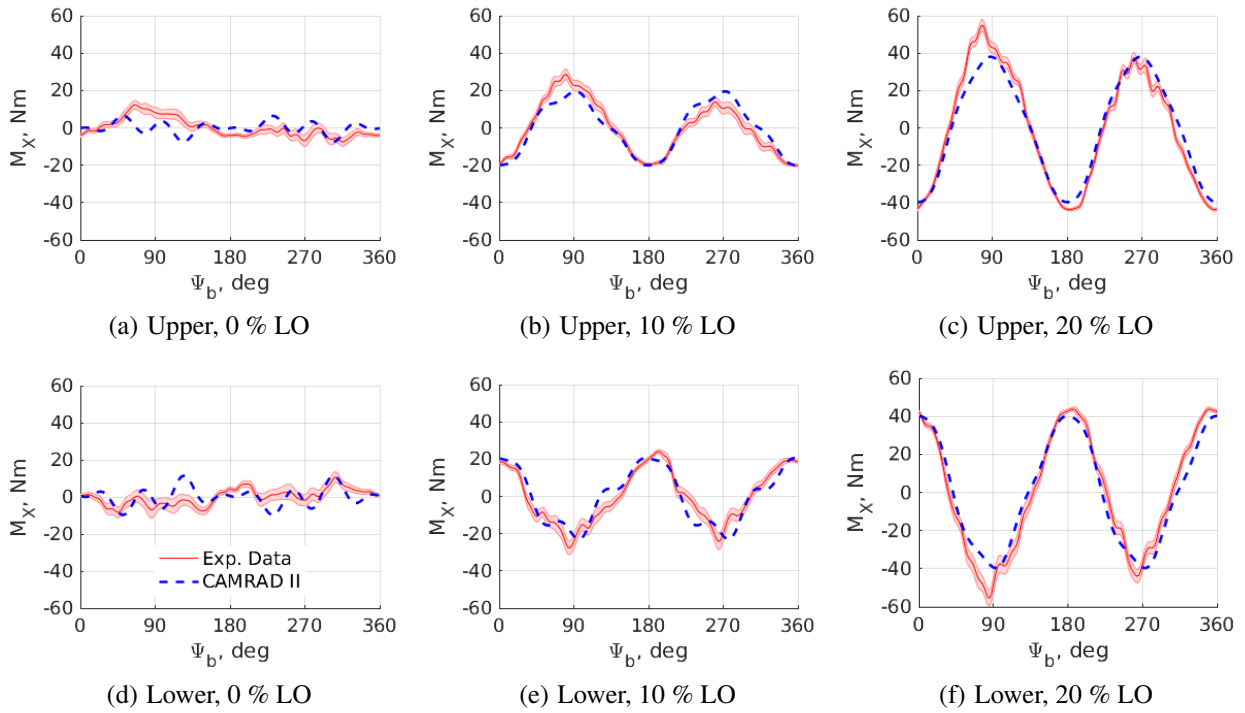


Fig. 14: Rotor rolling moments, M_x , (mean removed) at $\Theta_0 = 8^\circ$, $\mu = 0.31$, and $\Phi = 0^\circ$ for three different lift offsets.

lift offset (see Fig. 13 (c) and (f)) because of the 2/rev magnitudes decreasing for an improved lift offset setting.

The phase and magnitude of the hub rolling moments correlated well with the measurements; see Fig. 14. While there were only small magnitudes of mostly even harmonics present at zero lift offset condition, the 2/rev magnitudes increased consistently with larger lift offset, resulting in rising individual upper and lower rotor hub rolling moments; see also Fig. 19. This happened because the resulting thrust vector was further shifted to the advancing side with increasing lift offset (see Fig. 5) resulting in an increasing 2/rev response for a two-bladed rotor in the fixed frame. The total coaxial system rolling moment (not shown here), which was almost zero for the shown test condition because the upper and lower rotor rolling moments were out of phase, resulted from the superposition of both the upper and the lower rotor. Trim was achieved with torque balanced rotors and nominally zero total roll moment.

Note that uneven harmonics were not predicted by the current 2-by-2 bladed coaxial rotor analytical model because they were not induced by aerodynamic sources at the blades, and any other mechanically induced or transmitted vibrations (that may occur in the test rig) cannot be predicted by this model. Hence, for reasons of clarity the uneven harmonics were omitted in the frequency domain for both analysis and experiments; see Figs. 15–20.

Harmonic hub load content is shown with individual harmonic load coefficients from vibratory data normalized by each rotor's mean thrust coefficient C_T . Because the trim procedure targeted constant upper rotor collectives, as previously shown by Feil et al. [20], varying lift offsets also resulted in different blade loadings. Hence, by this normalization the results do not include effects of varying blade loadings but they focus on the dependencies on varying lift offset.

The trends of both drag and side forces correlated well with the experiments for both the 2/rev and the 4/rev results (see Figs. 15 and 16), although the amplitudes were significantly underpredicted except for the 4/rev in drag. The 4/rev in drag, that can at least in part be attributed to rotor–rotor interferences and multiples of the 2/rev, showed decreasing magnitudes with increasing lift offset and progressively steeper slopes for greater advance ratios. This nearly linear trend with varying lift offset resulted again from off-loading the retreating side. Increasing 4/rev magnitudes with increasing advance ratio resulted from the higher wind tunnel speeds. The predicted 4/rev characteristics in the side forces were similar to the 4/rev drag characteristics but were underpredicted compared to the measurements by a factor of around 2. This may at least in part be referred to the load cell dynamics that had a strong influence on the in-plane forces around the fourth harmonics. Also, the test stand dynamics from the experimental setup were different in the longitudinal and lateral directions, which could contribute to the discrepancy between longitudinal and lateral force dynamics. The numerics as well as the experiments

suggested that a minimum occurred for the 2/rev magnitude in drag at a certain lift offset. This drag minimum shifted to greater lift offsets with increasing advance ratio.

The thrust harmonics (see Fig. 17) showed the same magnitudes and trends in analysis and experiment. They were accurately predicted with relatively small underpredictions of the 4/rev, mostly at high speeds. Both the upper and the lower rotor showed decreasing 2/rev magnitudes with increasing lift offset. At low speeds, this trend reached a minimum in the 2/rev magnitude and increased again with larger lift offsets. The changing trend (or slope) in the 2/rev characteristics at very high lift offsets and low speeds (i.e., $LO > 15\%$ for $\mu = 0.21$) shown in Fig. 17 resulted from the retreating blade already being aerodynamically completely off-loaded and further off-loading the blade at this specific advance ratio was therefore disadvantageous from a loads perspective. In this case, the retreating blade was forced to produce negative lift to reach the targeted rolling moment, or lift offset, respectively. Figure 8 also showed that the effect of lift offset was not beneficial for the performance (L/D_e) at such low forward flight speeds where a minimum of the 2/rev thrust harmonics occurred.

An increasing advance ratio increased the resulting 2/rev thrust harmonics of this 2-by-2 bladed rotor because of the increased relative velocity on the advancing side and the reduced velocities on the retreating blade. Also, the apparent 1/rev characteristics in the angle of attack variation (see Fig. 12) were equivalent to the 2/rev characteristics in the hub loads for this two-bladed rotor because the angle of attack is shown for the reference blade only and the hub loads result from both blades accordingly; see e.g., Fig. 17. Increasing the lift offset off-loads the retreating side and results, in general, in more evenly distributed angles of attack over the rotor disk. By that it also improves the rotor efficiency at high advance ratios; see Figs. 7 and 8.

While at low speeds ($\mu \approx 0.2 - 0.3$) the upper and the lower rotor 2/rev thrust harmonics were approximately of the same magnitude, at high speeds the upper rotor 2/rev magnitude was significantly greater relative to the lower rotor. Upper and lower rotor 2/rev thrust diverged because at higher forward flight speeds greater parts of the upper rotor wake went past the lower rotor disk (because of the heavily skewed wake) and resulted in a varying asymmetric aerodynamic interaction between the coaxial rotors, inducing less vibrations on the lower rotor relative to the upper. This is a similar effect to the thrust sharing reversal that was observed from hover to faster forward flight [20]. Also, the current 2/rev thrust characteristics were previously analyzed by Schmaus and Chopra [22] using a different approach and at a lower collective. The effect of diverging upper and lower rotor 2/rev thrust magnitudes was insignificant and therefore not analyzed in their work. This outcome suggested that this effect increased with larger blade loading, e.g., collective pitch.

The 4/rev thrust characteristics (that are in general caused by rotor–rotor interactional aeromechanics of a 2-by-2-bladed coaxial rotor system) showed nearly constant

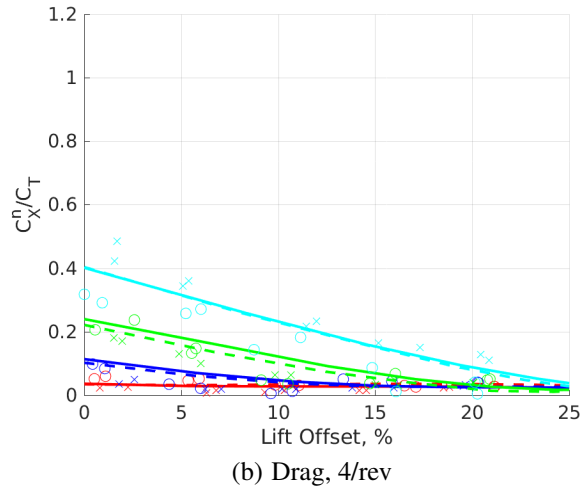
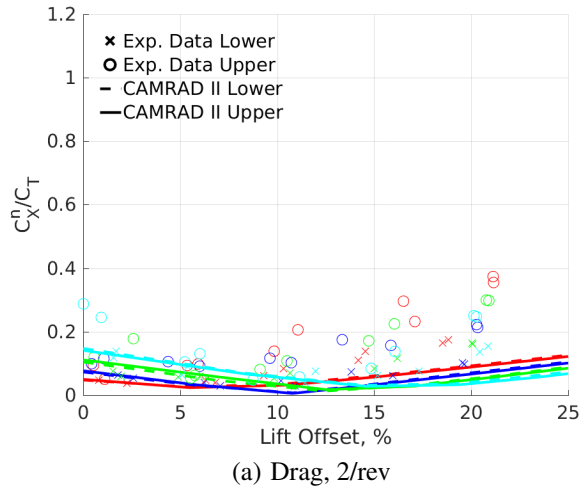


Fig. 15: Drag coefficient magnitudes of upper and lower rotor 2/rev and 4/rev harmonics over lift offset at $\Theta_0 = 8^\circ$ and $\Phi = 0^\circ$ for multiple advance ratios.

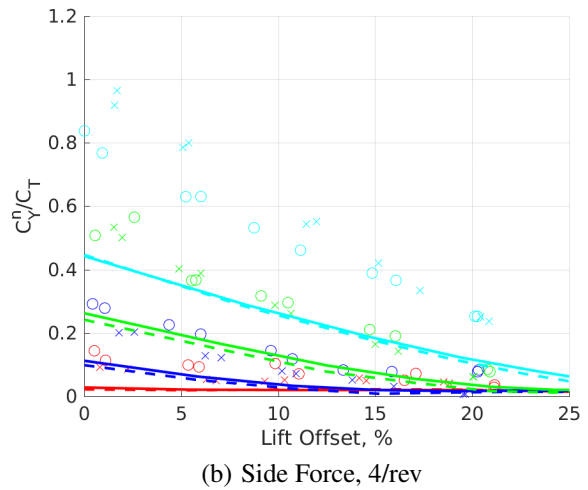
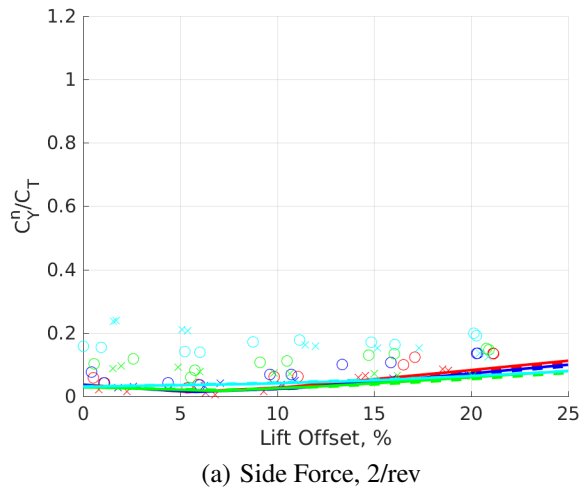


Fig. 16: Side force coefficient magnitudes of upper and lower rotor 2/rev and 4/rev harmonics over lift offset at $\Theta_0 = 8^\circ$ and $\Phi = 0^\circ$ for multiple advance ratios.

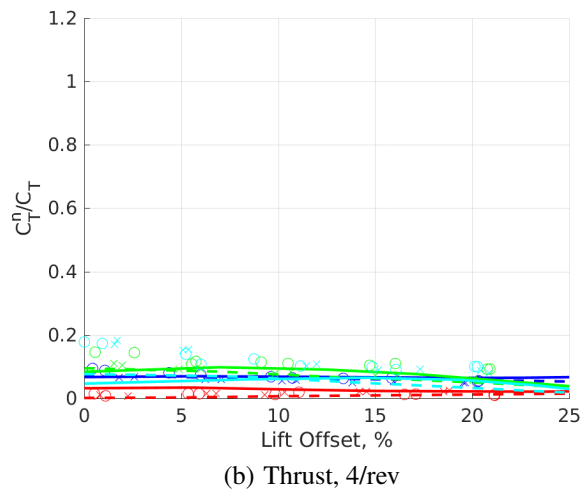
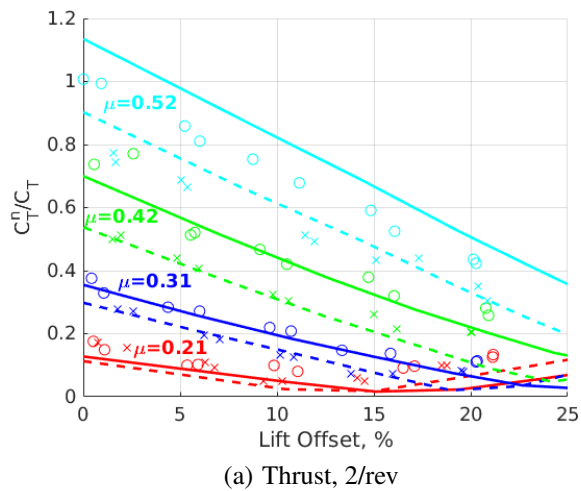
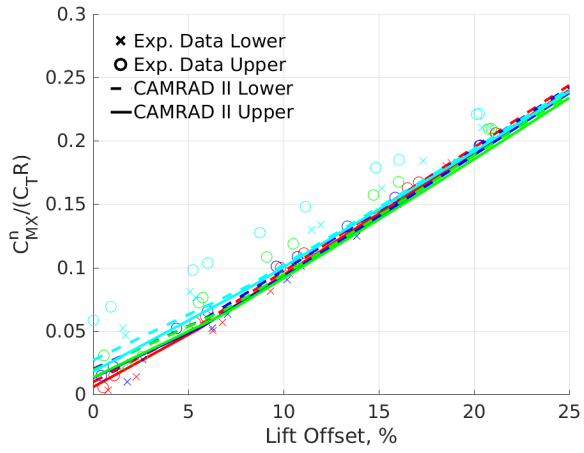
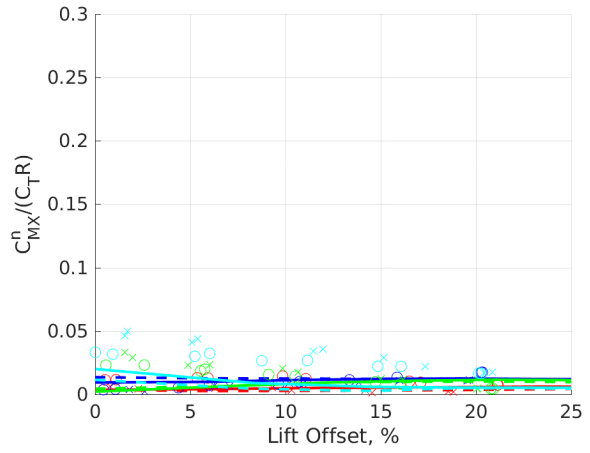


Fig. 17: Thrust coefficient magnitudes of upper and lower rotor 2/rev and 4/rev harmonics over lift offset at $\Theta_0 = 8^\circ$ and $\Phi = 0^\circ$ for multiple advance ratios.

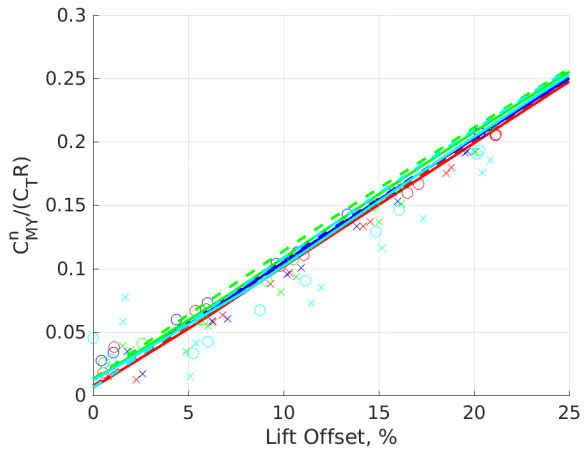


(a) Pitching Moment, 2/rev

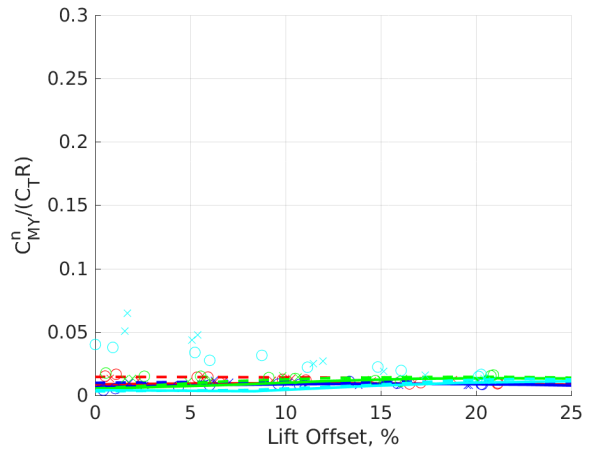


(b) Pitching Moment, 4/rev

Fig. 18: Pitching moment coefficient magnitudes of upper and lower rotor 2/rev and 4/rev harmonics over lift offset at $\Theta_0 = 8^\circ$ and $\Phi = 0^\circ$ for multiple advance ratios.

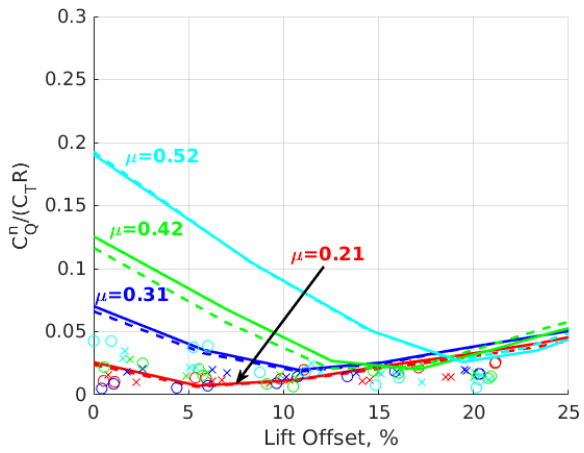


(a) Rolling Moment, 2/rev

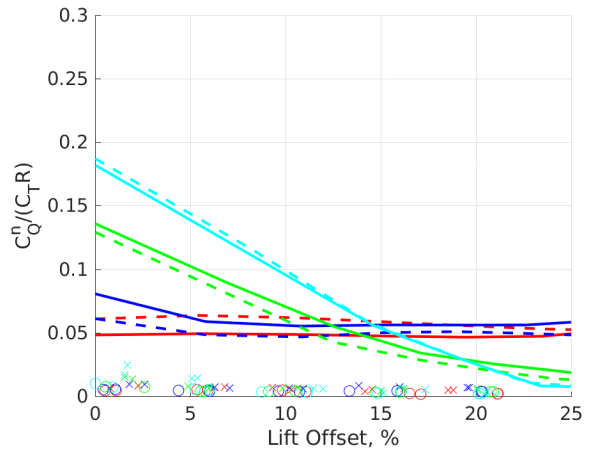


(b) Rolling Moment, 4/rev

Fig. 19: Rolling moment coefficient magnitudes of upper and lower rotor 2/rev and 4/rev harmonics over lift offset at $\Theta_0 = 8^\circ$ and $\Phi = 0^\circ$ for multiple advance ratios.



(a) Torque, 2/rev



(b) Torque, 4/rev

Fig. 20: Torque coefficient magnitudes of upper and lower rotor 2/rev and 4/rev harmonics over lift offset at $\Theta_0 = 8^\circ$ and $\Phi = 0^\circ$ for multiple advance ratios.

magnitudes for varying lift offsets and for both rotors; see Fig. 17. According to this result, the interference effects did not significantly change with off-loading the retreating blades.

Individual upper and lower rotor hub pitching and rolling moment harmonics are shown in Figs. 18 and 19. Both show equivalent magnitudes and trends compared to the measured values. Pitching and rolling moments 2/rev magnitudes increased nearly linearly with greater lift offset because of the resulting lift vector being further shifted to the advancing side of each rotor. For example, the rolling moment was maximal when the blades were at the advancing and retreating sides over the rotor disk and it was minimal when the blades were located at the nose and the tail sections; see Fig. 14. 4/rev magnitudes showed only minor variations with changing lift offset or advance ratio, with constantly low magnitudes over the range of analyzed and tested conditions.

The torque magnitudes (see Fig. 20) matched the experiments primarily at low speeds ($\mu = 0.21$) for the 2/rev response and otherwise overpredicted the experiments, particularly at low lift offset conditions with high advance ratios. At low lift offset condition, the experiments suggested that there was only a minor dependency from advance ratio on the 2/rev characteristics in torque, whereas CAMRAD II predictions showed significantly increasing magnitudes with greater wind speeds. The 2/rev torque, arising due to a variation in blade drag over the azimuth, decreases with increasing lift offset because of the favorable angle of attack distribution; see Fig. 12. The overprediction of torque may at least in part be explained by the respective elasticities of the drive train in the experimental setup. 4/rev torque harmonics were also overpredicted by the analysis. CAMRAD II predicted similar trends in 4/rev compared to the 2/rev harmonics. Increasing magnitudes resulted from greater advance ratios at low lift offsets, and reduced magnitudes for increasing lift offset, particularly at high advance ratios.

Effect of rotor–rotor phasing

Figure 21 shows the definition of the rotor–rotor phase angle, Φ , in this coaxial rotor system. An increasing phase angle shifts the first blade crossing from $\Psi_b = 0^\circ$ at zero rotor–rotor phasing ($\Phi = 0^\circ$) to higher blade azimuth angles, Ψ_b . For a 2-by-2 bladed coaxial rotor system, the first blade crossing happens at the rotor–rotor phasing angle $\Psi_b = \Phi$, the second at $\Psi_b = \Phi + 90^\circ$, the third at $\Psi_b = \Phi + 180^\circ$ and the fourth at $\Psi_b = \Phi + 270^\circ$. Zero azimuth was defined to be aligned with the tail-boom section, i.e., opposite the approaching flow. For a 2-by-2 bladed coaxial configuration, the rotor–rotor phasing may be varied between 0° and 45° .

The individual upper, lower, and total coaxial system rolling moments are shown in Fig. 22 for the three rotor–rotor phase angles that were tested in the wind tunnel. Note

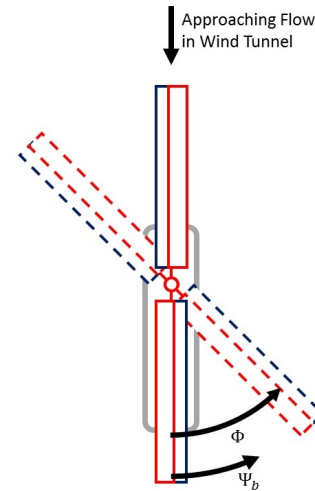


Fig. 21: Rotor–rotor phase angle definition, also showing dummy fuselage from experiments.

that measurements with phase angle variation were only taken for $\Theta_0 = 6^\circ$ and $\mu = 0.31$, which is why the following results corresponding to the effect of rotor phasing are all shown for this collective and advance ratio. Results from the numerical analysis showed the same trends and magnitudes as the experiments for all tested phase angles; see Fig. 22.

At zero inter-rotor phasing the upper rotor showed positive peak rolling moments while the lower rotor had negative peaks at the same azimuth effectively counteracting the upper rotor rolling moment. For increasing phase angles, the individual phases were shifted accordingly to higher Ψ_b for the upper rotor and to lower Ψ_b for the lower rotor; see Fig. 22. At $\Phi = 45^\circ$, the superposition of the upper and lower rotor rolling moments maximally increased the total coaxial system response, with the upper and lower positive and negative peaks being in phase with each other, resulting in increased 2/rev harmonics amplitudes of the total coaxial system rolling moment. However, the 2/rev rolling moment magnitude of the individual upper and lower rotors was the same with varying rotor–rotor phase as the 2/rev amplitude of each individual rotor primarily depended on the tested lift offset condition; see Fig. 14.

Figure 23 shows the resulting total coaxial system 2/rev roll moment harmonics magnitudes for increasing rotor–rotor phasing and for five lift offset conditions from zero to 21% LO. Analytical results included ten varying phase angles in steps of 5° that were connected with a spline for visualization purposes. Again, the effect of lift offset increasing the 2/rev rolling moment harmonics became obvious. Furthermore, the increasing 2/rev magnitudes with increasing rotor–rotor phasing that was observed in Fig. 22 is shown in more detail in Fig. 23.

Figure 24 shows both the upper and the lower rotor blade path at $0.9R$ over one rotor revolution for three different rotor–rotor phasings and at zero and high ($\approx 19\%$) lift offset. Note that for an evaluation of the upper and lower rotor clearance, the respective blade crossings are shown

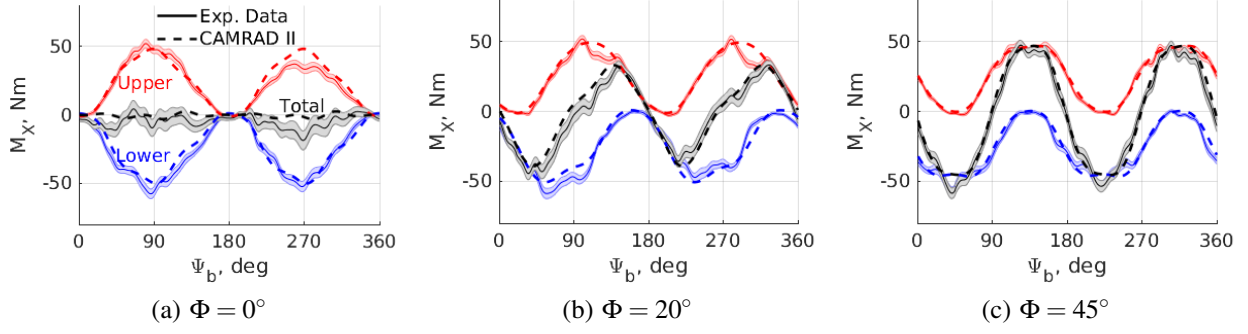


Fig. 22: Upper, lower and (total) coaxial system rolling moments, M_X , at $\Theta_0 = 6^\circ$, $\mu = 0.31$, and $LO \approx 16\%$ for three different rotor–rotor phase angles, Φ .

as vertical dashed lines and the azimuth angles of both rotors were defined according to Ψ_b that is shown in Fig. 21. Figure 24 shows that an increasing lift offset resulted in an off-loading of the retreating side and an increased loading on the advancing side (see Fig. 12) that yielded increasing blade deflections on the advancing side and reduced deflections on the retreating side of each rotor, thus reducing the tip clearance.

The critical blade crossing was at the fourth crossing at $\Psi_b = \Phi + 270^\circ$, where the lower blade was flapped in upward direction and the upper blade was flapped in downward direction; see Fig. 24. An increasing phase angle slightly affected the resulting blade path because of changing transient loads during blade crossing [25], and the respective blade crossings location changed to larger azimuth for an increasing phase angle, which also affected the resulting tip clearance at each blade crossing, e.g. at maximum phasing, $\Phi = 45^\circ$, the third crossing was at nearly the same clearance compared to the fourth crossing; see Figure 24 (c).

In Fig. 25 (a) the resulting coaxial rotor blade tip clearance at the critical blade crossing is shown over lift offset for three phase angles, and in Fig. 25 (b) for $\Phi = 0^\circ$ and the range of advance ratios that was tested. Tip clearance was normalized according to

$$\Delta z_{\text{tip}}^{\text{red.}} = \Delta z_{\text{tip}} \frac{C_{T, \text{mean, zero LO}}^{\text{total}}}{C_{T, \text{mean}}^{\text{total}}} \quad (3)$$

with $\Delta z_{\text{tip}} = z_{\text{tip}}^U - z_{\text{tip}}^L$ being the resulting tip clearance and the ratio between mean total coaxial thrust coefficient at zero lift offset, $C_{T, \text{mean, zero LO}}^{\text{total}}$, relative to the equivalent thrust coefficient at varying lift offset, $C_{T, \text{mean}}^{\text{total}}$. By reducing the data with the individual thrust characteristics the shown results for the tip clearance are independent of changes in rotor thrust with varying lift offset (when trimmed to a constant Θ_0) and render it possible to analyze the pure effect of lift offset. This dependence of thrust on lift offset was discussed previously in Ref. [20].

Figures 25 (a) and (b) show that the resulting rotor–rotor tip clearances reduced with increasing lift offset. The

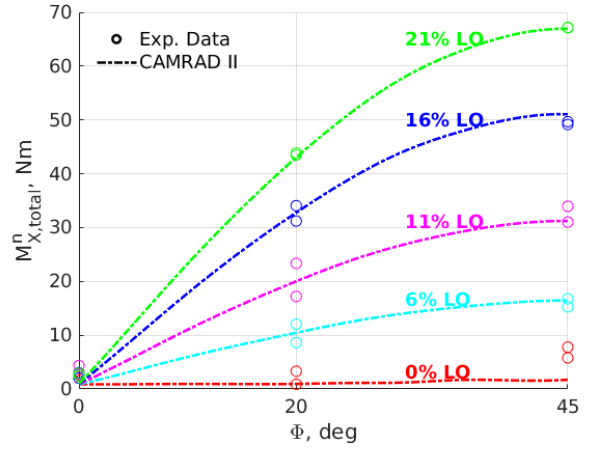


Fig. 23: 2/rev harmonic magnitudes of (total) coaxial system rolling moments as a function of inter-rotor phasing at $\Theta_0 = 6^\circ$, $\mu = 0.31$, and for various LO.

changing peak locations with varying rotor phasing as illustrated in Fig. 24 in the time domain also resulted in larger rotor–rotor clearance with greater phase angles, seen from both the analysis and the experiments; see Fig. 25 (a). This is because at higher lift offset conditions the resulting deflection peak locations were dominated by the advancing and the retreating sides of each blade, and with increasing phase angle the critical fourth blade crossing steadily moved further to higher Ψ_b ; see Fig. 24. Hence, an increasing rotor–rotor phase angle increased the minimum tip clearance, with greater influence at larger lift offsets. While keeping in mind that the total coaxial rolling moment 2/rev characteristics significantly increased with larger rotor–rotor phasing, this effect could consciously be used for such closely spaced coaxial rotors to get greater tip separations, especially at large lift offset operation.

Figure 25 (b) improves previously shown results from Feil et al. [20] by adaptation of the blade root flap bending stiffness validated at the 1st flap frequency, as described previously in the modeling approach; see Fig. 4. The predicted clearances showed the same trends and magnitudes compared to the experiments, with slight overpredictions at high lift offsets.

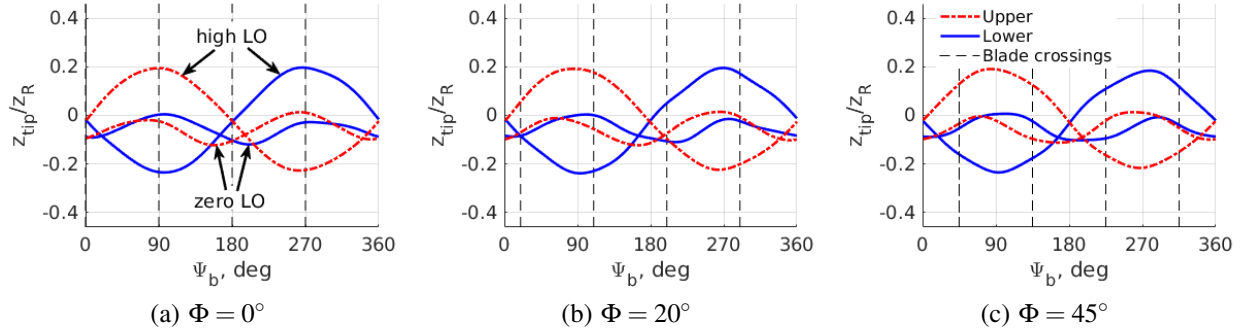


Fig. 24: Upper and lower rotor blade deflection predictions at 90% radius for three different rotor-rotor phase angles at $\Theta_0 = 6^\circ$, $\mu = 0.31$, and for zero and high ($\approx 19\%$) LO. Vertical dashed lines depicting blade crossings.

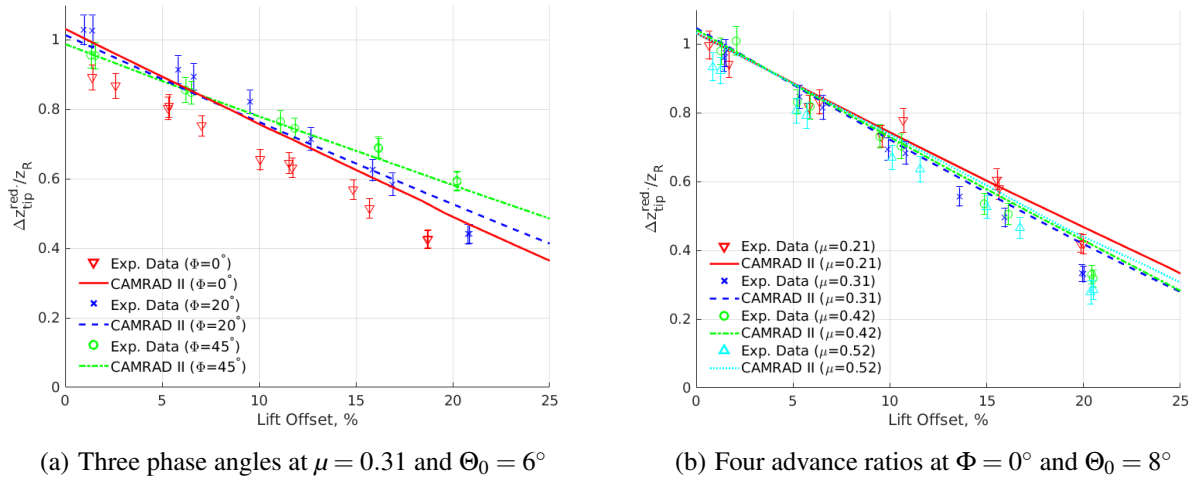


Fig. 25: Coaxial rotor tip clearance at 90% radius at the fourth blade crossing for (a) three different rotor-rotor phase angles and for (b) four advance ratios, for increasing LO.

By reducing the data according to Eq. 3 it is shown that an increasing advance ratio only slightly affected the resulting tip clearance. Previous analysis [20] suggested increased clearance with higher advance ratio only because of the thrust dependency on lift offset, i.e., because the thrust or blade loading was significantly affected by lift offset if the rotor was trimmed to a fixed collective pitch.

5. CONCLUSIONS

Coaxial rotorcraft aeromechanics were analyzed and evaluated by means of a comprehensive analysis. The model was validated by extensive experimental data from hover and wind tunnel tests for varying lift offsets between zero and 25% and advance ratios up to 0.52. This paper continued previous efforts [20,21] and focused on the progressing validation of the numerical model and the analysis of the 2m-diameter coaxial rotor test rig in terms of blade dynamics, control loads and hub loads. Effects such as rotor-rotor phasing and resulting tip clearance for this lift-offset rotor configuration were also investigated.

The following specific conclusions have been drawn:

- The rotor blade structural dynamics of the CAMRAD II model were calibrated by the first three flap, the first lag and the first torsion non-rotating natural frequencies. Modeling of control system elasticities reduced the first torsional frequency of the upper and the lower rotor according to their respective control system geometries and stiffness.
- The evaluation of the performance in terms of lift-to-drag ratio showed that, in general, the faster the wind tunnel was operated the more advantageous was a greater lift offset.
- Pitch link loads correlated well with the experiments in both magnitudes and phase. Off-loading the retreating blade, i.e., a greater lift offset significantly reduced the magnitude of the first harmonic pitch link load.
- Good agreement between the numerical model and the experiments were found in the vibratory rotor thrust, pitching and rolling moments. Rotor drag also showed good correlations with a slight underprediction in the 2/rev magnitude, and the side force predictions showed the correct trends but with underpre-

diction of the 2/rev and 4/rev magnitudes. Vibratory rotor torque was overpredicted, which is attributed to the finite stiffness of the drive train components in the experiments that were not accounted for in the modeling.

- Rotor thrust 2/rev decreased with greater lift offset due to the off-loading of the retreating blade. Increasing asymmetric aerodynamic interactions at higher advance ratios resulted in greater 2/rev magnitudes at the upper rotor relative to the lower rotor.
- Individual rotor hub rolling moments correlated well with the experimental data in both magnitude and phase for variable lift offsets and rotor-rotor phase angles. Resulting 2/rev (total) coaxial system rolling moments increased significantly with larger phase angles because of the individual upper and lower rotor moment peak locations being shifted relative to each other with varying phase angle.
- Inter-rotor phasing slightly affected the blade tip paths. Because of the changing azimuthal locations of the blade crossings with varying phase angle, modified coaxial rotor-rotor clearance was found from both analysis and experiments. Larger phasing increased the minimum clearance, with more pronounced effects at high lift offset operation. It also resulted in greater 2/rev magnitudes of the (total) coaxial system rolling moment.

Future work includes further improvements of the modeling capabilities by using, e.g., non-rigid drive train models, and to examine the effects of the aerodynamic sources such as blade vortex interaction effects on the rotors vibratory loads for such closely spaced rotors. The validated comprehensive analysis will also be used to model compound rotorcraft configurations with auxiliary propulsors. The current work on the interactional aerodynamics and dynamics of a model-scale high-advance-ratio coaxial rotor intends to further the understanding of such configurations, and therefore will also be of interest for current and future designs that use thrust compounding.

ACKNOWLEDGEMENTS

The authors would like to thank Dr. Jayant Sirohi and Dr. Christopher Cameron from the University of Texas for providing the experimental data from extensive hover and wind tunnel testing, as well as Dr. Joseph Schmaus at the University of Maryland for providing the VR-12 airfoil tables.

REFERENCES

[1] Ormiston, R. A., "Revitalizing Advanced Rotorcraft Research - and the Compound Helicopter," *Journal of the American Helicopter Society*, Vol. 61, 2016.

[2] Johnson, W., Elmore, J. F., Keen, E. B., Gallaher, A. T., and Nunez, G. F., "Coaxial Compound Helicopter for Confined Urban Operations," American Helicopter Society Specialists' Conference on Aeromechanics Design for Vertical Lift, San Francisco, CA, USA, January 20–22, 2016.

[3] Leishman, J. G., *Principles of Helicopter Aerodynamics*, Cambridge University Press, 2nd ed., 2006.

[4] Bagai, A., "Aerodynamic Design of the X2 Technology Demonstrator Main Rotor Blade," Proceedings of the American Helicopter Society 64th Annual Forum, Montreal, QC, Canada, April 29–May 1, 2008.

[5] Walsh, D., Weiner, S., Arifian, K., Bagai, A., Lawrence, T., and Blackwell, R., "Development Testing of the Sikorsky X2 Technology™ Demonstrator," Proceedings of the American Helicopter Society 65th Annual Forum, Grapevine, TX, USA, May 27–29, 2009.

[6] Blackwell, R. and Millott, T., "Dynamic Design Characteristics of the Sikorsky X2 TD Aircraft," Proceedings of the American Helicopter Society 65th Annual Forum, Montreal, QC, Canada, April 29 – May 1, 2008.

[7] Walsh, D., Weiner, S., Arifian, K., Lawrence, T., Wilson, M., Millot, T., and Blackwell, R., "High Airspeed Testing of the Sikorsky X2 Technology Demonstrator," Proceedings of the American Helicopter Society 67th Annual Forum, Virginia Beach, VA, USA, May 3–5, 2011.

[8] Coleman, C. P., "A Survey of Theoretical and Experimental Coaxial Rotor Aerodynamic Research," Tech. Rep. 3675, NASA Ames Research Center, 1997.

[9] Ramasamy, M., "Hover Performance Measurements Toward Understanding Aerodynamic Interference in Coaxial, Tandem, and Tilt Rotors," *Journal of the American Helicopter Society*, Vol. 60, 2015.

[10] Juhasz, O., Syal, M., Celi, R., Khromov, V., Rand, O., Ruzicka, G., and Strawn, R., "Comparison of Three Coaxial Aerodynamic Prediction Methods Including Validation with Model Test Data," *Journal of the American Helicopter Society*, Vol. 59, 2014.

[11] Johnson, W., "Influence of Lift Offset on Rotorcraft Performance," Tech. Rep. 215404, NASA Ames Research Center, 2009.

[12] Yeo, H. and Johnson, W., "Investigation of Maximum Blade Loading Capability of Lift-Offset Rotors," *Journal of the American Helicopter Society*, Vol. 59, 2014.

[13] Passe, B., Sridharan, A., and Baeder, J., "Computational Investigation of Coaxial Rotor Interactional Aerodynamics in Steady Forward Flight," 33rd AIAA Applied Aerodynamics Conference, AIAA Aviation, Dallas, TX, USA, June 22–26, 2015.

- [14] Singh, R., Kang, H., Bhagwat, M., Cameron, C. G., and Sirohi, J., "Computational and Experimental Study of Coaxial Rotor Steady and Vibratory Loads," 57th AIAA/ASCE/AHS/ASC Structures, Structural Dynamics, and Materials Conference, AIAA SciTech, San Diego, CA, USA, January 4–8, 2016.
- [15] Uehara, D. and Sirohi, J., "Quantification of Swirl Recovery in a Coaxial Rotor System," Proceedings of the American Helicopter Society 73rd Annual Forum, Fort Worth, TX, USA, May 9–11, 2017.
- [16] Cameron, C. G., Karpatne, A., and Sirohi, J., "Performance of a Mach-Scale Coaxial Counter-Rotating Rotor in Hover," *Journal of Aircraft*, Vol. 53, 2016.
- [17] Cameron, C., Uehara, D., and Sirohi, J., "Transient Hub Loads and Blade Deformation of a Mach-Scale Coaxial Rotor in Hover," 56th AIAA/ASCE/AHS/ASC Structures, Structural Dynamics, and Materials Conference, AIAA SciTech, Kissimmee, FL, USA, January 5–9, 2015.
- [18] Cameron, C., Karpatne, A., and Sirohi, J., "Performance and Vibratory Hub Loads of a Mach-Scale Coaxial Rotor in Hover," Proceedings of the American Helicopter Society 70th Annual Forum, Montreal, QC, Canada, May 20–22, 2014.
- [19] Cameron, C. G. and Sirohi, J., "Performance and Loads of a Model Coaxial Rotor Part I: Wind Tunnel Testing," Proceedings of the American Helicopter Society 72nd Annual Forum, West Palm Beach, FL, USA, May 17–19, 2016.
- [20] Feil, R., Rauleder, J., Hajek, M., Cameron, C. G., and Sirohi, J., "Computational and Experimental Aeromechanics Analysis of a Coaxial Rotor System in Hover and Forward Flight," Proceedings of the 42nd European Rotorcraft Forum, Lille, France, September 6–8, 2016.
- [21] Feil, R., Rauleder, J., and Hajek, M., "Aeromechanics Analysis of a Coaxial Rotor System in Hover and High-Advance-Ratio Forward Flight," 34th AIAA Applied Aerodynamics Conference, AIAA Aviation, Washington, DC, USA, June 13–17, 2016.
- [22] Schmaus, J. and Chopra, I., "Validation of Predicted Vibratory Loads of a Coaxial Rotor at High Advance Ratios with Wind Tunnel Test Data," Proceedings of the 42nd European Rotorcraft Forum, Lille, France, September 6–8, 2016.
- [23] Schmaus, J. and Chopra, I., "Performance and Loads of a Model Coaxial Rotor Part II: Prediction Validations with Measurements," Proceedings of the American Helicopter Society 72nd Annual Forum, West Palm Beach, FL, USA, May 17–19, 2016.
- [24] Schmaus, J. and Chopra, I., "Aeromechanics for a High Advance Ratio Coaxial Helicopter," Proceedings of the American Helicopter Society 71st Annual Forum, Virginia Beach, VA, USA, May 5–7, 2015.
- [25] Cameron, C. G., Feil, R., Sirohi, J., and Rauleder, J., "Measurement of Transient Loads and Blade Deformation in a Coaxial Counter-Rotating Rotor," Proceedings of the American Helicopter Society 73rd Annual Forum, Fort Worth, TX, USA, May 9–11, 2017.
- [26] Ho, J. C., Yeo, H., and Bhagwat, M., "Validation of Rotorcraft Comprehensive Analysis Performance Predictions for Coaxial Rotors in Hover," *Journal of the American Helicopter Society*, Vol. 62, 2017.
- [27] Yeo, H., Bosworth, J., Acree, C. W., and Kreshock, A. R., "Comparison of CAMRAD II and RCAS Predictions of Tiltrotor Aeroelastic Stability," Proceedings of the American Helicopter Society 73rd Annual Forum, Fort Worth, TX, USA, May 9–11, 2017.
- [28] Johnson, W., "Technology Drivers in the Development of CAMRAD II," American Helicopter Society Aeromechanics Specialists Conference, San Francisco, CA, USA, January 19–21, 1994.
- [29] Bagai, A. and Leishman, J. G., "Rotor FreeWake Modeling Using a PseudoImplicit Technique Including Comparisons with Experimental Data," *Journal of the American Helicopter Society*, Vol. 40, 1995.
- [30] Leishman, J. G., Bhagwat, M. J., and Bagai, A., "Free-Vortex Filament Methods for the Analysis of Helicopter Rotor Wakes," *Journal of Aircraft*, Vol. 39, 2002.
- [31] Lim, J. W., Yu, Y. H., and Johnson, W., "Calculation of Rotor BladeVortex Interaction Airloads Using a Multiple-Trailer Free-Wake Model," *Journal of Aircraft*, Vol. 40, 2003.
- [32] Johnson, W., *Rotorcraft Aeromechanics*, Cambridge Aerospace Series, Cambridge University Press, 2013.